Unaccounted impacts of diterpene emissions on atmospheric aerosol loadings

Ana Yañez-Serrano

ana.yanez@idaea.csic.es

Institute of Environmental Assessment and Water Research (IDAEA)

Josep Penuelas

CSIC, Global Ecology Unit CREAF-CSIC-UAB, Cerdanyola del Vallès 08193, Catalonia, Spain https://orcid.org/0000-0002-7215-0150

Oriol Jorba

Barcelona Supercomputing Center (BSC) https://orcid.org/0000-0001-5872-0244

Frans Graeffe

Institute for atmospheric and earth system research (INAR/physics), University of Helsinki; Helsinki, 00014, Finland https://orcid.org/0000-0001-7304-4651

Melissa Meder

University of Helsinki

Olga Garmash

Department of Chemistry

Yanjun Zhang

Atmospheric Composition Research

Haiyan Li

Harbin Institute of Technology

Yuanyuan Luo

Institute for atmospheric and earth system research (INAR/physics), University of Helsinki; Helsinki, 00014, Finland

Arnaud Praplan

Finnish Meteorological Institute https://orcid.org/0000-0002-9944-3084

Heidi Hellen

Finnish Meteorological Institute https://orcid.org/0000-0001-7022-3857

Siegfried Schobesberger

Department of Applied Physics, University of Eastern Finland https://orcid.org/0000-0002-5777-4897

Lejish Vettikkat

University of Eastern Finland https://orcid.org/0000-0001-6808-5643

Steven Thomas

Institute for Atmospheric and Earth System Research (INAR)

Theo Kurtén
University of Helsinki https://orcid.org/0000-0002-6416-4931
Ditte Taipale
University of Helsinki
Efstratios Bourtsoukidis
The Cyprus Institute https://orcid.org/0000-0001-5578-9414
Alex Guenther
University of California, Irvine https://orcid.org/0000-0001-6283-8288
Mikael Ehn
University of Helsinki https://orcid.org/0000-0002-0215-4893

Article

Keywords:

Posted Date: November 13th, 2024

DOI: https://doi.org/10.21203/rs.3.rs-5407662/v1

Additional Declarations: There is **NO** Competing Interest.

Unaccounted impacts of diterpene emissions on atmospheric aerosol loadings

Ana Maria Yáñez-Serrano[1,2,3], Josep Peñuelas[2,3], Oriol Jorba[4], Frans Graeffe[5], Melissa Meder[5], Olga Garmash[6], Yanjun Zhang[7], Haiyan Li[5], Yuanyuan Luo[5], Arnaud Praplan[7], Heidi Hellén[7], Siegfried Schobesberger[8], Lejish Vettikkat[8], Steven Thomas[5,7], Theo Kurten[9, 5], Ditte Taipale[5], Efstratios Bourtsoukidis[10], Alex Guenther[11], and Mikael Ehn[5].

[1]{IDAEA-CSIC, 08034, Barcelona, Spain}
[2]{CREAF, E08193 Bellaterra (Cerdanyola del Vallès), Catalonia, Spain}
[3]{CSIC, Global Ecology Unit, CREAF-CSIC-UAB, E08193 Bellaterra (Cerdanyola del Vallès), Catalonia, Spain}
[4]{Barcelona Supercomputing Center - Centro Nacional de Supercomputación, Barcelona, Spain}
[5] {Institute for Atmospheric and Earth System Research, Faculty of Science, University of Helsinki, Helsinki, 00014, Finland}
[6] {Department of Chemistry, University of Copenhagen, 2100, Copenhagen, Denmark}
[7] {Atmospheric Composition Research, Finnish Meteorological Institute, Helsinki, 00101, Finland}
[8] {Department of Technical Physics, University of Eastern Finland, 70211 Kuopio, Finland}
[9]{ Department of Chemistry, Faculty of Science, University of Helsinki, Helsinki, 00014, Finland}
[10]{Climate and Atmosphere Research Center (CARE-C), The Cyprus Institute, Nicosia, Cyprus}
[11]{Department of Earth System Science, University of California, Irvine, CA, USA}

Abstract

Diterpenes ($C_{20}H_{32}$) are commonly found in trees, but their emissions into the atmosphere were previously considered unlikely due to their low volatility. Consequently, they have been disregarded in atmospheric chemistry processes. Recent improvements in sampling and analytical instrumentation have enabled the detection and quantification of diterpenes in the gas phase. However, the atmospheric implications of these emissions, including their potential to form secondary organic aerosol (SOA), are not well understood. This study provides the first quantification of kaurene emissions and their potential contribution to secondary organic aerosol (SOA) formation. Here, we incorporate all available emission measurements of kaurene (the most measured diterpene species) and findings from laboratory investigations of SOA formation into a global chemistry transport model to quantify the importance of diterpenes on SOA loads in the atmosphere. Chamber experiments revealed an SOA yield of 4% to 7%, demonstrating the rapid gas-to-particle phase transition, while global kaurene emissions, estimated at 5.1 Tg yr^{-1}, contribute to an SOA burden of 0.005 Tg. Our findings suggest that diterpenes contribute to SOA formation, establishing new links to the biosphere-atmosphere interactions that are increasingly important due to climate warming.

Secondary organic aerosol (SOA) is the dominant type of fine-mode aerosol mass[1], yet large scale models generally underpredict the magnitude of observed organic aerosol[2–6]. These aerosols, formed from the oxidation of volatile organic compounds (VOCs), have profound impacts on the global radiation balance, either directly by scattering[7,8] and absorbing solar radiation[9], or indirectly by impacting cloud and rain formation processes[10,11]. Furthermore, they can boost global primary productivity up to 25% for some ecosystems via diffuse radiation fertilization[12]. Therefore, it is essential to understand which VOCs are emitted, how large those emissions are, and what fraction of a given VOC will ultimately be able to form SOA.

Isoprenoids are a group of biogenic VOCs (BVOC) that have been identified as the dominant sources of SOA globally[1,13,14]. These compounds can protect against oxidative damage at the (sub-)cellular level and can serve as signalling compounds within plant-plant and plant-insect interactions, as well as at the plant and ecosystem levels, providing protection against biotic and abiotic stress[15]. Isoprenoids can be emitted *de novo,* from recently photosynthesized carbon, like isoprene (C_5) and some monoterpenes (C_{10}) or be released from storage pools like most monoterpenes and sesquiterpenes (C_{15}). Despite diterpenes (C_{20}) being constituents of many plants' essential oils[16,17], they were until recently thought not to be emitted into the gas phase due to their low volatility [18], and thus have never been considered relevant for atmospheric chemistry.

Diterpenes have important roles inside plants, such as growth regulators, providing an essential building block for chlorophyll (a diterpene conjugate), and playing crucial roles in ecological interactions between plants and other organisms, such as signalling and defence against herbivores in the form of oleoresins[18,19]. There is a wide range of diterpene molecular species (S.I. Sec. 1), and some reports have pointed that emissions are temperature dependent[20–22] and derived from storage pools[21,23]. These studies also point out that diterpenes are most likely emitted from plants with a highly active secondary metabolism[21]. Nevertheless, considerable gaps still exist in understanding the diterpene emissions from vegetation given the small number of plant species measured for diterpene emissions and the scarce ambient observations available up to date.

Methodological improvements in both sampling and detection have enabled observations of diterpenes in the gas phase. Ambient air mixing ratios of diterpenes have been reported from a rural site in Amazonia and two temperate forests (Landes forest in France and the Rocky mountains in the USA) ranging from 19 ppq to 2 ppt[24,25]. Diterpene emissions from plants have been recently detected from mosses[26], temperate[27] and boreal conifer trees[20,28], grasses[22], broadleaf trees[29], Mediterranean shrubs[21,30] and soil emissions from permafrost[31]. Additionally, diterpene emissions were observed during cooking with herbs [32]. In order to give a proper overview, we have performed a literature review on all available diterpene measurements to date. We selected only kaurene emissions and derived basal emission factors (needed for BVOC emission modelling) for those studies that did not report it. This literature synthesis can be found in the Supplementary Information (SI section 2).

For this study, we focus on *ent*-kaurene as it is the most studied diterpene. While our conclusions may not apply equally to all diterpenes, it offers strong evidence for their overall significance. When emitted into the atmosphere, all C_{20} compounds are expected to impact aerosol loading simply due to their mass, similar to other large highly reactive isoprenoids such as the sesquiterpenes (C_{15})[33,34]. Very recently, kaurene ozonolysis was shown to produce a wide range of different highly oxygenated products able to condense and form SOA[35]. Importantly, due to its exocylic double bond[36], kaurene is expected to be among the least reactive diterpenes, hence using kaurene as a representative C_{20} species establishes only the lower limit for the atmospheric impact of diterpenes, indicating that the cumulative impact of all diterpenes is higher. In addition, diterpenes could be a part of the so-called missing OH reactivity due to their terpene nature as suggested for different environments[37,20].

There is a substantial lack of data available to refine current emission models[38] and aerosol formation from diterpenes. To address these knowledge gaps, we performed the first experimental SOA chamber aerosol forming potential studies for kaurene where we were able to obtain the first kaurene SOA yield. This new result, in conjunction with improved emission estimates, was used in the Multiscale Online Non-hydrostatic AtmospheRe CHemistry model (MONARCH) to assess the potential impact of kaurene emissions on the atmospheric SOA loading.

Results

SOA chamber experiments to determine the kaurene SOA formation yield. We performed chamber experiments using authentic kaurene standard (see Methods for details) to simulate the relevant atmospheric processes. Kaurene and ozone were injected into the chamber, resulting in kaurene oxidation by ozone, but to some extent also by hydroxyl radicals (OH) formed from the ozone-alkene reactions. Also in the atmosphere, kaurene will be oxidized by both O_3 and OH, and therefore the conditions can be assumed roughly representative of atmospheric conditions. We added ammonium sulphate aerosols to the chamber to act as seeds for condensation of the oxidation products. The experiments were performed at loadings ranging from 0.11 to 11 ppb, and the best estimate derived for the SOA molar yield from kaurene oxidation by O_3 and OH is 4-7% (Figure 1). This yield was lower than anticipated based on typical values observed for other terpenes, where larger molecular sizes often correlate with higher SOA yields[33,39–41]. However, it is well known that the VOC structure has an important role, as e.g. monoterpene SOA yields vary from negligible to several tens of percent[41].

Kaurene has one exocyclic double bond, which is not a favourable structure for autoxidation which may supress the formation of highly oxygenated species. To some extent, it can be compared to the monoterpene β-pinene, which also has a similar exocyclic double bond and typically shows a much lower SOA yield from ozonolysis than its counterpart α-pinene[40], where the double bond is endocyclic. This comparison suggests that kaurene falls within the lower range of SOA yields for diterpenes, compared to diterpenes with endocyclic double bonds, like e.g. cembrene. Our SOA yield estimates are in agreement with the gas-phase kaurene oxidation measurements performed under the same conditions, where a highly oxygenated organic molecules (HOM) molar yield of a few percent was reported[35].

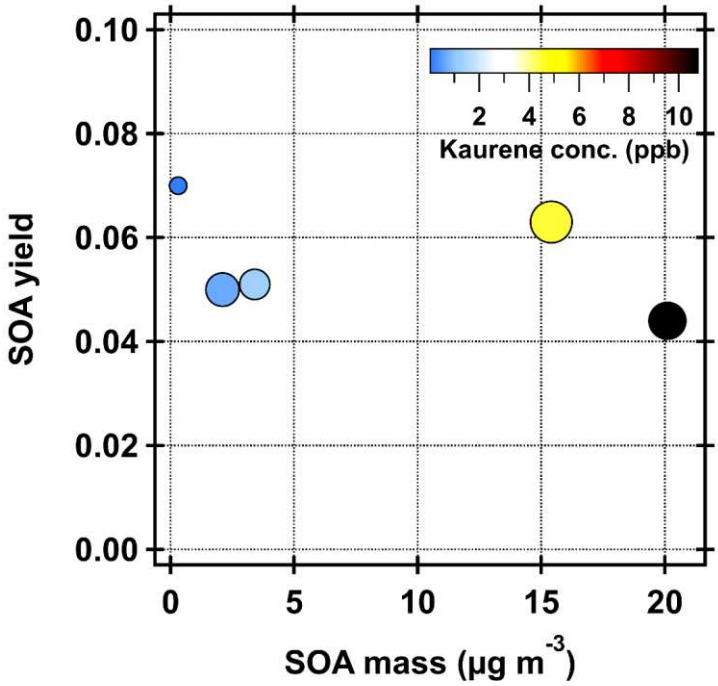

Figure 1: Measured SOA molar yield as a function of formed SOA mass. Colouring of the markers is based on the average kaurene concentration (range 0.11 to 11 ppb) and the size of markers is based on the average ammonium sulphate seed concentration (ranging from 5.8 to 42 µg m^{-3}) in the chamber for the corresponding SOA steady state time period.

Global simulations of kaurene emissions and the production of kaurene SOA. We used the global chemical transport model, MONARCH[42–48], to estimate global emissions and SOA burdens of kaurene for the year 2018. In this work, MONARCH was adapted to consider emissions of kaurene from vegetation as provided by the literature synthesis given in SI sect. 2, and the SOA formation yield from the experimental chamber results performed for this study.

BVOC emissions were computed online within MONARCH using the Model of Emissions of Gases and Aerosols from Nature biogenic emissions (MEGANv2.04: Guenther et al., 2006[49]). A new biogenic VOC species was added to account for kaurene emissions. The model estimates BVOC emission based on plant functional types (PFT). From our literature synthesis on all available measurements of kaurene emissions by vegetation[20,21,52,22–25,28,30,50,51], we were able to derive average basal emission factors (standardised emissions rates at 30ºC) for kaurene for needle leaf trees[28,50], shrubs[21,30], broadleaf trees[29] and grasses[22] (see Table SI. 2.2).

The basal emission factors reported exhibit significant variability. Moreover, there is limited data available for grasses and broadleaf trees, with only one study reporting values for each. Despite the evident need for more measurements, we have applied the average basal emission factor for needle leaf and shrubs species, and the one available value for grasses and broadleaf trees, respectively. Furthermore, for grass and broadleaf trees, we used the sum of diterpenes, not only kaurene. While we

acknowledge the inherent uncertainty in this assumption, it presents the best approach for our simulations, which are prone to considerable uncertainty due to both scarcity of data on kaurene emissions and their potential for atmospheric aerosol formation. At the same time, it allows us to investigate the impacts of kaurene vegetation emissions on atmospheric aerosol loadings.

The percentage of VOC emissions from vegetation is an important computational assumption. For instance, for isoprene, monoterpenes and sesquiterpenes, the model assumes that 100% of vegetation emits these compounds (albeit at different rates depending on PFT, as different vegetation types are assumed to have very different potentials to emit these compounds). Since the precise fraction of vegetation emitting kaurene is unknown (i.e. we do not know if all plant species emit kaurene), we have established one very conservative scenario with only 10% of vegetation emitting kaurene, and a less conservative scenario of 50% of vegetation emitting kaurene, to understand the sensitivity of the system. The consequent emission factors for kaurene employed in this study are provided in Table 1.

Table 1: Selected basal emission factors for kaurene for the different PFTs available in the model for kaurene emissions at a global scale. The values are expressed in micrograms per square meter per hour ($\mu g\ m^{-2}\ hr^{-1}$). The basal emission factors used for α-pinene, β-pinene and β-carophyllene are also shown for comparison. The large difference in the distributions between different PFT for kaurene compared to other terpenes may indicate that that diterpene emissions are very different than other terpenes, or that the limited emission observations cause large uncertainties.

PFT	Kaurene	α-pinene	β-pinene	β-caryophyllene
Grass/crops	5.4	2	1.5	0.9
Broadleaf	0.024	180	90	30
Needle leave tree	162.8	450	300	60
Shrub + bush	8.81	200	100	45

The global annual emission for kaurene is estimated as 5.1 Tg yr^{-1}, in contrast to 424.8 Tg yr^{-1} for isoprene, 90.3 Tg yr^{-1} for monoterpenes or 13.5 Tg yr^{-1} for sesquiterpenes, as derived from the same modeling framework (for more details see SI. Figs. 3.2.1., 3.2.2. and 3.2.3.). For comparison, our isoprene emission estimate aligns closely with previous literature estimates[53].

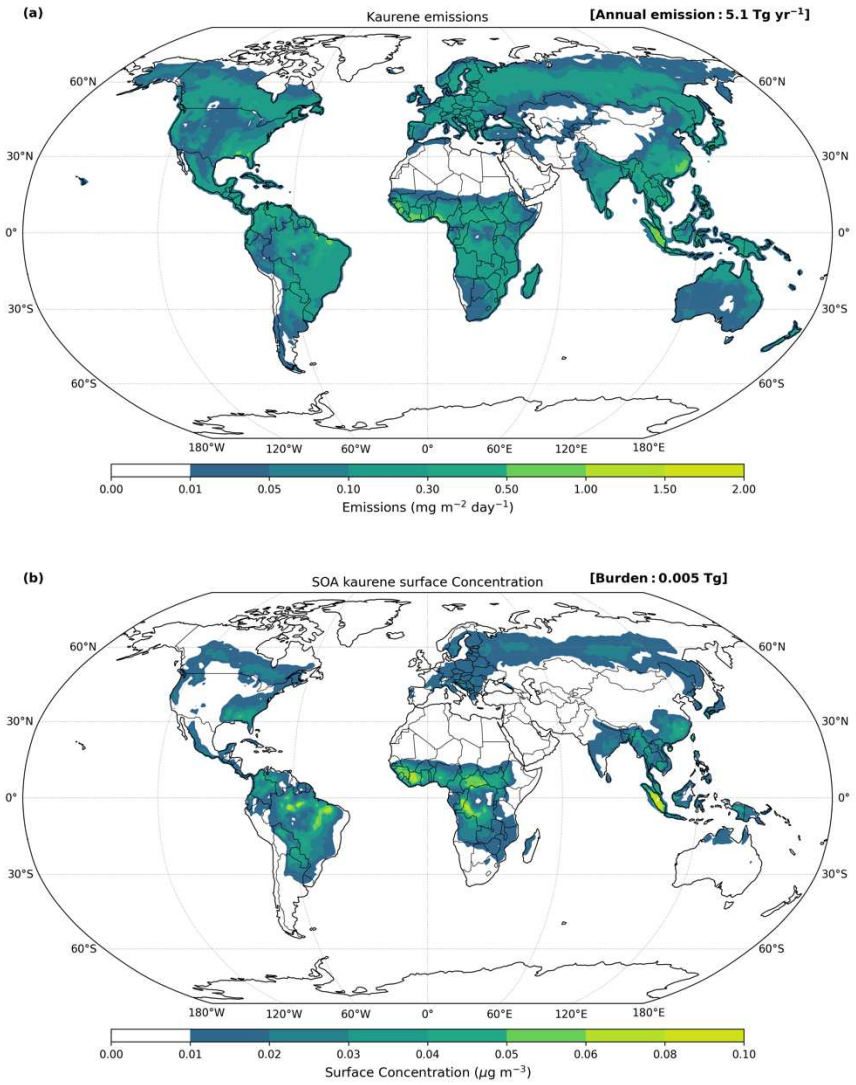

Figure 2: Annual average (a) kaurene emission rates [mg m^{-2} day^{-1}] and (b) SOA kaurene surface concentration [µg m^{-3}] estimates for 2018 assuming only 10% of the vegetation emits kaurene.

The emission of kaurene exhibits significant variability both spatially and seasonally (Fig. 2a and Fig. SI 3.1.1 and 3.1.2.), being strongly influenced by the emission factors integrated into the model (Table 1). Globally, peak emissions typically occur in summer. Tropical rainforests demonstrate a relatively consistent emission pattern throughout the year, with heightened emissions observed in Southeast Asia and Southwestern Africa. Conversely, the boreal region and Southeastern US experience elevated kaurene emissions during the growing season. These emissions suggest that even if the basal emission of needle leaf trees is overestimated, kaurene emissions are still dominant in tropical forests, where needle leaf trees are not present or in very little abundance[54].

To derive the first estimates of the potential effect of the contribution of kaurene to SOA formation, we analyze the MONARCH results that were adapted to the experimental data obtained by the controlled SOA formation experiments. Thus, we considered 7% SOA yield for kaurene, 1% for isoprene, 10% for monoterpenes and 20 % for sesquiterpenes. The yields for isoprene[55–57], monoterpenes[40,56] and sesquiterpenes[56,58,59] were approximated in this way given the wide range of yields reported in literature.

	Precursor emission (Tg yr^{-1})	Burden (Tg)	Source (Tg yr^{-1})	Dry dep. (Tg yr^{-1})	Wet dep. (Tg yr^{-1})	Total dep. (Tg yr^{-1})	Lifetime (days)
SOA kaurene (10%/50% veg. emits)	5.1/25.5	0.005/0.025	0.36/1.8	0.07/0.36	0.29/1.43	0.36/1.81	5.0
SOA isoprene	424.8	0.066	4.25	0.62	3.62	4.24	5.6
SOA monoterpenes	90.3	0.125	9.03	1.72	7.31	9.02	5.1
SOA sesquiterpenes	13.5	0.042	2.71	0.45	2.25	2.70	5.7

Table 2. Global annual average vegetation emission and SOA burden (mass in the atmosphere of a specific SOA species in Tg) for kaurene, isoprene, monoterpenes and sesquiterpenes for the year 2018. Annual depositions, production and lifetime are also reported. Kaurene results are reported for the two simulations available, one scenario with only 10% of the vegetation emitting kaurene and a second scenario where 50% of the vegetation emits kaurene. See S.I. Table 3 for comparison of isoprene, monoterpenes and sesquiterpenes with other studies.

The average aerosol mass in the atmosphere, i.e., the burden) of SOA from kaurene vegetation emission for 2018 was 0.005 Tg with a SOA production of 0.36 Tg yr^{-1}, which is lower than the SOA burden from monoterpenes (0.125 Tg) or sesquiterpenes (0.042 Tg). Given that we only consider a single diterpene species, this result suggests that the real SOA burden of diterpenes is expected to be larger as some diterpenes may have larger SOA yields than kaurene, summing up to a potentially considerable SOA contributor globally. Following the kaurene emission trends, the highest kaurene SOA production globally takes place in northern hemispheric summer, although year-around production of SOA occurs around the tropics, especially in South West Africa and Indonesia. Kaurene SOA production follows a similar regional trend as kaurene vegetation emissions (Figs. 2 and SI 3.1.3 and 3.1.4.).

The simulated global emission for the sum of monoterpenes is 90.3 Tg yr^{-1}. With a 10% SOA yield, this would lead to 9 Tg yr^{-1} of SOA produced from monoterpenes. This value, together with the average SOA burden of 0.125 Tg, makes the average lifetime of the monoterpene SOA just over 5 days, which is consistent with literature[60,61]. As a comparison, kaurene SOA lifetime derived from the simulation stands at 5 days consistently.

Discussion and conclusions

This study provides the first estimate for kaurene ozonolysis SOA yield. Leveraging the estimated yield of HOM[35] and considering the low volatility of kaurene and its oxidation products, our findings suggest that kaurene influences SOA formation, which was not previously considered. Through experimental data, we model the global vegetation emission of kaurene and SOA production, incorporating empirical constraints for kaurene SOA formation, namely SOA yields and emission rates. Our analysis yields a global estimate of kaurene emissions totalling 5.1 Tg yr^{-1} for the year 2018. Additionally, we we estimate the global kaurene SOA production to be 0.36 Tg yr^{-1} for 2018 based on experimentally determined SOA yield.

The major uncertainty in this study lies in the provided emission factors for the different plant functional types, necessitating caution with the simulated kaurene vegetation emission and kaurene SOA burden. The uncertainty arises not only from the scarcity of studied plant species but also from the extremely high variability in the reported emission magnitudes, with differences of up to three orders of magnitude. The proportion of kaurene emission factors among the different PFTs is different than for other more known terpenes. This could be due to three reasons: 1) kaurene emissions might be fundamentally different from other terpenes, 2) the non-needle-leaf tree emission factors might be

highly underestimated, or 3) the needle leaf tree emission factor might be highly overestimated. In the latter case, it is crucial to note that the needle leaf tree emission factor is an average of all measured needle leaf tree species, and this basal emission may have been overestimated for certain needle leaf tree species, such as *C. Japonica* and *C. Obtusa*, as their basal emission factors differ by up to three orders of magnitude higher from other plant species. Nevertheless, a recent study reported extremely high emissions for *C. Obtusa*[23], suggesting this species may have a very high emission capacity for kaurene. This underscores the necessity for comprehensive screening of kaurene emissions across different plant species. While the uncertainties of emissions are large, the emission factors used in this study are based on values reported in the literature, and exhibit equally high variability as monoterpenes[62].

Our study represents an important step towards quantifying diterpene emissions and investigating their impacts on SOA production. Kaurene is only one of the many diterpene species, and thus total diterpene emissions will be larger than the single species investigated here. In fact, for some tree species, such as Norway Spruce[20], kaurene emissions were not detected, but several other diterpenes appeared to dominate the emission profile. Furthermore, the molecular structure of kaurene suggests it should be less reactive than other diterpenes given its exocyclic bond. Therefore, the SOA yield for other diterpenes than kaurene is expected to be higher, amplifying their impact on the SOA budget and emphasizing the need for further investigation into these compounds.

In this study, we demonstrate that kaurene emission by vegetation can influence global SOA formation, and thus must be considered in atmospheric models. Our finding helps towards understanding the so-called *unmeasured compounds*, as diterpenes (including kaurene) are not often measured largely because of their high molecular weight, and can in part explain the 'missing OH reactivity'[37]. Furthermore, aerosols formed from kaurene ozonolysis may contribute to elucidating the unidentified fraction of Biogenic SOA[63]. However, it is imperative to enhance the precision of diterpene emission and SOA yield estimates. Such observations need to take into account a broader pool of plant species, including tropical forest species, for which there are no reported emission, but ambient air observations are available and indicate diterpene emissions by vegetation.

Here we took the first steps towards quantifying global kaurene vegetation emissions and their impact on SOA formation. We experimentally derived the first kaurene SOA yield of 4-7% from chamber experiments, and their potential to form SOA. The modelled SOA burden of 0.005 Tg from this one diterpene species suggests that this is a compounds group with potentially large implications on atmospheric reactivity and SOA production. The SOA-forming potential of kaurene suggests that current global SOA models may be underestimating the contribution of biogenic sources, particularly in regions where kaurene-emitting plants are abundant. These findings could inform future air quality models and guide conservation efforts in regions where kaurene-emitting plants play a significant role in local atmospheric chemistry, and add an important piece of information for studying biosphere-atmosphere interactions in a warming world.

METHODS

1. Controlled kaurene SOA experiments

Kaurene ozonolysis experiments were conducted in a 2 m^3 Teflon (FEP, supplied by Vector Foiltec, Germany) chamber, the COALA chamber at the University of Helsinki, Finland. An authentic pure solid kaurene standard was purchased from OLChemIm Ltd., Olomouc. Czech Republic. The total flow was around 36 L min^{-1} consisting of purified air, varying amounts of O_3 and diterpene ent-kaurene, and 80 nm inorganic seed particles comprised of ammonium sulphate (AS). The chamber was operated at room temperature (26 $\pm$ 1 ºC) and under dry condition (RH <1%). The composition of VOCs was measured with the Vocus Proton Transfer Reaction Time of Flight mass spectrometer (Vocus PTR-ToF)[64]. The chemical composition of SOA was measured with a Long ToF Aerosol Mass Spectrometer (LToF-AMS)[65]. In addition, we had a custom-built scanning mobility particle sizer (SMPS) to measure

the particle number size distribution. Based on the SMPS data, we also calculated area and volume concentrations. The SOA, ammonium sulphate (AS) and total particle mass concentrations were calculated by using the total particle volume from the SMPS combining it with the density and SOA to AS ratio measured with the AMS. More information on this experiment set up can be found in Luo et al., 2022[35]. This approach, rather than directly using the measured mass concentrations from the AMS, was utilized since the collection efficiency of the AMS varies as a function of the ratio between organics and AS[66]. The details of the chamber facility, instruments, and experiments are found elsewhere[67].

All instruments sampled the chamber air continuously, and the input into the chamber was varied (Fig. 3) to achieve different concentrations and ratios of kaurene and O_3. The O_3 concentrations ranged from ~70 to ~110 ppb for different experiments, and the kaurene concentration was at most ~20 ppb. Seed aerosols were added at different times in order to initiate condensation onto aerosols rather than chamber walls, which is usually the dominant sink for low-volatility vapours. The injection of kaurene was one of the most challenging parts of the experiments due to its low volatility. Gas-phase kaurene was introduced into the chamber by flushing nitrogen (N_2) through a vial containing the solid kaurene, and the flow was subsequently directed into the chamber. In addition, a heater was placed under the vial to promote the evaporation of kaurene. During the experiments, the vial's bottom temperature stayed below 45 ºC, except for the last experiment day when the vial reached a temperature around 60 ºC. Already at low heating, the solid kaurene had melted to liquid form, but we did not see indications of decomposition of the kaurene from the heating in any of our mass spectra. Variable levels of kaurene in the chamber were achieved, either by turning the heater on and off or changing the flow rate of the N_2 carrier gas, which was controlled with a mass flow controller (MKS, G series, Andover, MA, USA). Due to the low volatility of kaurene, residual amounts were introduced into the chamber also when no active addition was performed, presumably due to evaporation from surfaces in the tubing and chamber.

2. SOA yield estimation

As we used a steady state chamber, the SOA yield cannot simply be calculated by dividing the measured SOA mass with an amount of reacted VOC, as would be the case in batch-mode chambers. Instead, we estimate the SOA yield using a simple box model of our chamber, changing the effective SOA yield (as the only free parameter) to match the measured SOA. Next, a short description of the box model is presented.

We assume that the SOA is formed from low volatility vapors (LVOCs) produced from the kaurene + ozone reactions, formed with a molar yield of $yield_{LVOC}$. The sink of these LVOCs is condensation onto the AS-seed and the chamber walls. At steady state, when the sources and sinks are equal, we can write the LVOC concentration as:

$$LVOC = \frac{[O_3]*[kaurene]*k_{O_3+kau}*yield_{LVOC}}{k_{wall}+CS},$$

where k_{O3+kau} is the reaction rate coefficient for kaurene and ozone, k_{wall} is the wall loss rate of LVOC, and CS is the condensation sink to the AS-seed. The CS was simply estimated from the measured mass concentration, scaled linearly using the relation $CS = 0.0015 \frac{s^{-1}}{\frac{\mu g}{m^3}} * m_{tot}$, where m_{tot} is the total particle mass concentration, based on Peräkylä et al. (2020) who used an identical approach in our chamber. k_{wall} is estimated as 1/400 s^{-1} for our chamber, based also on Peräkylä et al. (2020). The change in the SOA mass concentration is now governed by the source (condensation of LVOCs) and the sink (flush-out from the chamber):

$$\frac{\Delta SOA}{\Delta t} = [LVOC] * CS * C_{m,LVOC} - SOA * k_{outflow},$$

where $k_{outflow}$ is the chamber flush-out, given as the reciprocal of the average chamber residence time (~36 min), and $C_{m,LVOC}$ is a conversion factor for converting the LVOC number concentration to mass

concentration. For $C_{m,LVOC}$, we assume that the mass of LVOCs to be on average 352 Da, which represents the mass of a $C_{20}H_{32}O_5$ molecule. The change in SOA can thus be modelled by:

$$\frac{\Delta SOA}{\Delta t} = [O_3] * [kaurene] * k_{O3+kau} * yiel \frac{d_{LVOC} * C_{m,LVOC} * CS}{CS + k_{wall}} - SOA * k_{outflow}$$

For every time step in the model, we used the measured kaurene, ozone and AS-seed concentrations. Therefore, only the concentration of SOA was modelled. A value of $0.5 \cdot 10^{-15} cm^3 s^{-1}$ was used for the reaction rate coefficient for kaurene + ozone, determined during these experiments, similar to other studies[20]. More details on how we derived such coefficient can be found elsewhere[35].

The $yield_{LVOC}$ corresponds to the molar yield of condensable vapors (LVOC). In our chamber, some fraction of these LVOC condenses onto the walls (typically around 20-30 %, based on calculations from Peräkylä et al. (2020), but in the atmosphere these would all contribute to SOA formation. The final SOA yield is normally defined as a mass yield, meaning that our molar yield needs to be multiplied by the mass increase, i.e. $yield_{SOA} = yiel \frac{d_{LVOC} * m_{LVOC}}{m_{kaurene}} = yield_{LVOC} * 1.29$. We note here that both $yield_{LVOC}$ and m_{LVOC} could be varied to match the measured SOA, but the $yield_{SOA}$ parameter only depends on their product, which means that it is independent of the exact choice of either. As such, the SOA yield is effectively the only free parameter in the model. An example of a simulated experiment is shown in Fig. 3. The SOA yields obtained for time periods where we had a stable SOA concentration in the chamber is presented in the same figure.

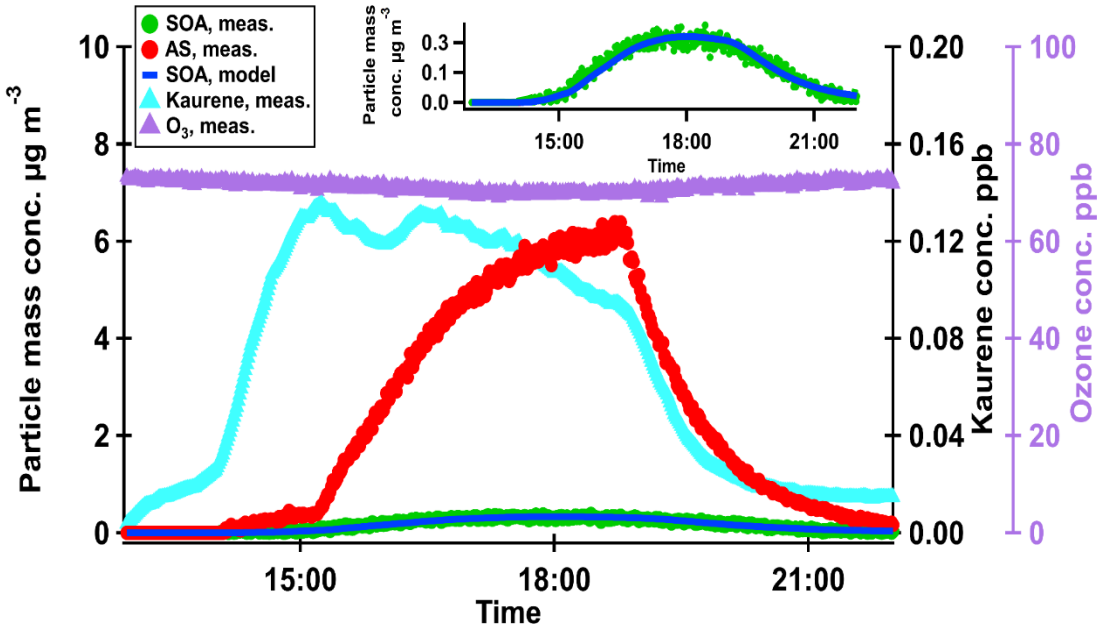

Figure 3. Yield experiment with the particle mass concentration on the y-axis for measured SOA (in green), ammonium sulphate-seed (in red) and modelled SOA concentrations (in blue), together with the concentration of kaurene on the right-axis and blue triangles and the concentration of ozone on the right-axis with purple triangles, from a day with $yield_{SOA} = 7\%$ The inset plot is zoomed in from the actual plot to see more clearly the match between measured and modelled SOA concentrations.

3. Model implementation

We have used the Multiscale Online Nonhydrostatic AtmospheRe CHemistry model (MONARCH)[42–48] to estimate emissions and SOA global burdens of kaurene. The simulations were conducted with MONARCH model, which was run at the global scale on a regular longitude-latitude grid of a global

domain at 0.7° x 0.5º horizontal resolution and on 48 hybrid sigma-pressure vertical levels. The year 2018 was simulated driven by the meteorology of the ERA5 reanalysis[68]. The anthropogenic emissions applied are based on the CAMS-GLOB-ANTv4.2 database[69], and the biomass-burning emissions were from the Global Fire Assimilation System v1.2 biomass-burning emissions (GFAS)[70]. Additionally, other meteorology-driven emissions are computed within MONARCH, such as mineral dust[57] and sea salt[56].

MONARCH is a fully on-line integrated system for mesoscale to global-scale applications developed at the Barcelona Supercomputing Center (BSC). MONARCH is designed to provide short to medium-range forecasts of atmospheric aerosols for a wide range of scales[71]. The model allows running both global and regional simulations with telescoping nests. As multiple choices of gas- and aerosol chemistry schemes can be selected in the model, here we describe the configuration used in this work. The gas-phase chemistry solves the carbon bond mechanism with extended chlorine chemistry (CB05)[72]. The model describes the lifecycle of dust, sea-salt, black carbon, organic matter (both primary and secondary), sulphate, ammonium, nitrate aerosols and non-speciated aerosols. While a sectional approach is used for dust and sea salt, a modal representation of the other aerosol species is adopted[47]. A simplified gas–aqueous–aerosol mechanism has been introduced in the module to account for the sulfur chemistry[47] and a simple scheme is used for the formation of secondary organic aerosols [60].

Organic aerosol is represented by a hydrophobic mode with atmospheric aging that transfers mass to a hydrophilic mode with a conversion lifetime of 1.15 days. Half of the primary emissions are emitted as hydrophobic species with an OM:OC (Ambient organic-mass-to-organic-carbon) ratio of 1.4, while the hydrophilic counterpart is emitted assuming an OM:OC ratio of 2.1. Marine primary organic emissions are neglected in our simulations. SOA contributions from biogenic, pyrogenic and anthropogenic sources are accounted for with fixed SOA yields adjusted to match results from more complex schemes[60] (e.g., volatility basis set). Half of the biogenic SOA is emitted directly in the aerosol phase to account for the near-field formation of SOA, while the rest describes the gas-phase SOA products that partitions to SOA with a conversion lifetime of 1 day[60].

Biogenic emissions are computed online using the Model of Emissions of Gases and Aerosols from Nature biogenic emissions (MEGANv2.04[49]), which is the available version for the MONARCH set up, and provided the uncertainties on kaurene emissions, the use of this more simplified MEGAN version is suitable. A new biogenic VOC species has been added to account for kaurene emissions. From the literature review we performed on kaurene vegetation emissions (SI sec 2) we have derived basal emission factors which have been separated into the four plant functional types used in MEGANv2.04 (see description in Table 1). The β-coefficient used for deriving basal emission factors was 0.15 $°C^{-1}$. This value was the average β-coefficient values reported in literature (a subset of the reviewed literature). Since both kaurene and β-pinene have an exocyclic double bond and due to the lack of experimental data on kaurene oxidation, we used β-pinene as a surrogate for kaurene for the MEGAN parameter where no information for kaurene was available within MEGANv2.04.

To provide first global estimates of the potential significance of kaurene contribution to SOA formation from the ozonolysis of kaurene, we extended the biogenic SOA production scheme in MONARCH[60] to kaurene adapting accordingly to the experimental data obtained by the controlled SOA formation experiments. Thus, we considered 7% SOA yield for kaurene, 1% for isoprene, 10% for monoterpenes and 20 % for sesquiterpenes. The yields for isoprene[55–57], monoterpenes[40,56] and sesquiterpenes[56,58,59] were approximated in this way given the wide range of yields reported in literature.

Data availability statement

The data is available upon request to the corresponding author.

Author Contribution Statement

Conceptualization: AMYS, JP, TK, DT, AG, ME

Investigation: AMYS, JP, OJ, FG, MM, OG, YZ, HL, YL, AP, DT, ME
Data curation: AMYS, OJ, DT, FG, HH, SS, LV, TS, EB, ME
Funding acquisition and administration: JP, OJ, ME
Methodology: AMYS, OJ, FG, OG, MM, ME
Visualization: AMYS, JP, OJ, FG, ME
Formal analysis: AMYS, OJ, FG, ME
Resources: AMYS, JP, OJ, ME
Supervision: AMYS, JP, ME
Writing original draft: AMYS, JP, FG, ME
Writing review & editing: All authors

Acknowledgements

AMYS acknowledges La Caixa Foundation Junior Leader retaining fellowship and Grant CEX2018-000794-S funded by MCIN/AEI/ 10.13039/501100011033, the support from the Consolidación Investigadora project (CNS2022-135757), her Ramon y Cajal grant (RYC2021-032519-I), and her Juan de la Cierva grant both awarded by the Spanish Research Agency. DT acknowledges The Academy of Finland (grant no. 307957). JP was supported by the Spanish Government grants PID2022-140808NB-I00 and TED2021-132627 B–I00 funded by MCIN, AEI/10.13039/501100011033 European Union Next Generation EU/PRTR. MM acknowledges the Niilo Helander Foundation and the Magnus Ehrnrooth Foundation. SS and LV Academy of Finland grant numbers 310682, 346371 and 357905. OJ acknowledges the support of the Department of Research and Universities of the Government of Catalonia via the Research Group Atmospheric Composition (code 2021 SGR 01550).

References

1. Jimenez, J. L. *et al.* Evolution of Organic Aerosols in the Atmosphere. *Science (80-.).* **326**, 1525–1529 (2009).

2. Bergman, T. *et al.* Description and evaluation of a secondary organic aerosol and new particle formation scheme within TM5-MP v1.2. *Geosci. Model Dev.* **15**, 683–713 (2022).

3. Tsigaridis, K. *et al.* The AeroCom evaluation and intercomparison of organic aerosol in global models. *Atmos. Chem. Phys.* **14**, 10845–10895 (2014).

4. Martin, S. T. *et al.* Sources and properties of Amazonian aerosol particles. *Rev. Geophys.* **48**, RG2002 (2010).

5. Heald, C. L. *et al.* Exploring the vertical profile of atmospheric organic aerosol: Comparing 17 aircraft field campaigns with a global model. *Atmos. Chem. Phys.* **11**, 12676–12696 (2011).

6. Spracklen, D. V. *et al.* Aerosol mass spectrometer constraint on the global secondary organic aerosol budget. *Atmos. Chem. Phys.* **11**, 12109–12136 (2011).

7. Artaxo, P. *et al.* The role of biogenic, biomass burning and urban pollution aerosol particles in controlling key atmospheric processes in Amazonia. (2013).

8. Kulmala, M. *et al.* Climate Feedbacks Linking the Increasing Atmospheric CO2 Concentration, BVOC Emissions, Aerosols and Clouds in Forest Ecosystems. in *Biology, Controls and Models of Tree Volatile Organic Compound Emissions* 489–508 (Springer, Dordrecht, 2013). doi:10.1007/978-94-007-6606-8_17.

9. Boucher, O. *et al.* Clouds and Aerosols. in *Climate Change 2013: The Physical Science Basis. Contribution of Working Group I to the Fifth Assessment Report of the Intergovernmental Panel on Climate Change (IPCC)* (eds. Stocker, T. F. et al.) 571–657 (Cambridge University Press, Cambridge UK and New York USA, 2013).

10. Makkonen, R. *et al.* Sensitivity of aerosol concentrations and cloud properties to nucleation and secondary organic distribution in ECHAM5-HAM global circulation model. *Atmos. Chem. Phys.* **9**, 1747–1766 (2009).

11. Kerminen, V. M., Lihavainen, H., Komppula, M., Viisanen, Y. & Kulmala, M. Direct observational evidence

linking atmospheric aerosol formation and cloud droplet activation. *Geophys. Res. Lett.* **32**, 1–4 (2005).

12. Rap, A. *et al.* Enhanced global primary production by biogenic aerosol via diffuse radiation fertilization. *Nat. Geosci.* **11**, 640–644 (2018).

13. McFiggans, G. *et al.* Secondary organic aerosol reduced by mixture of atmospheric vapours. *Nat. 2019 5657741* **565**, 587–593 (2019).

14. Glasius, M. & Goldstein, A. H. Recent Discoveries and Future Challenges in Atmospheric Organic Chemistry. *Environ. Sci. Technol.* **50**, 2754–2764 (2016).

15. Harrison, S. P. *et al.* Volatile isoprenoid emissions from plastid to planet. *New Phytol.* **197**, 49–57 (2013).

16. Judzentiene, A. & Kupcinskiene, E. Chemical Composition on Essential Oils from Needles of Pinus sylvestris L. Grown in Northern Lithuania. *http://dx.doi.org/10.1080/10412905.2008.9699413* **20**, 26–29 (2011).

17. Islam, M. T. *et al.* Therapeutic Potential of Essential Oils Focusing on Diterpenes. *Phyther. Res.* **30**, 1420–1444 (2016).

18. Keeling, C. I. & Bohlmann, J. Genes, enzymes and chemicals of terpenoid diversity in the constitutive and induced defence of conifers against insects and pathogens. *New Phytol.* **170**, 657–675 (2006).

19. Pelot, K. A. *et al.* Functional Diversity of Diterpene Synthases in the Biofuel Crop Switchgrass. *Plant Physiol.* **178**, 54 (2018).

20. Helin, A., Hakola, H. & Hellén, H. Optimisation of a thermal desorption-gas chromatography-mass spectrometry method for the analysis of monoterpenes, sesquiterpenes and diterpenes. *Atmos. Meas. Tech.* **13**, 3543–3560 (2020).

21. Yáñez-Serrano, A. M. *et al.* Volatile diterpene emission by two Mediterranean Cistaceae shrubs. *Sci. Rep.* **8**, 6855 (2018).

22. Vettikkat, L. *et al.* High emission rates and strong temperature response make boreal wetlands a large source of isoprene and terpenes. *Atmos. Chem. Phys.* **23**, 2683–2698 (2023).

23. Saito, T., Kusumoto, N. & Hiura, T. Relation of leaf terpene contents to terpene emission profiles in Japanese cedar (Cryptomeria japonica). *Ecol. Res.* **38**, 74–82 (2023).

24. Li, H. *et al.* Terpenes and their oxidation products in the French Landes forest: Insights from Vocus PTR-TOF measurements. *Atmos. Chem. Phys.* **20**, 1941–1959 (2020).

25. Yee, L. D. *et al.* Observations of sesquiterpenes and their oxidation products in central Amazonia during the wet and dry seasons. *Atmos. Chem. Phys.* **18**, 10433–10457 (2018).

26. von Schwartzenberg, K., Schultze, W. & Kassner, H. The moss Physcomitrella patens releases a tetracyclic diterpene. *Plant Cell Rep.* **22**, 780–786 (2004).

27. Matsunaga, S. N. *et al.* Monoterpene and sesquiterpene emissions from Sugi (Cryptomeria japonica) based on a branch enclosure measurements. *Atmos. Pollut. Res.* **2**, 16–23 (2011).

28. Fischer, L. *et al.* First eddy covariance flux measurements of semi-volatile organic compounds with the PTR3-TOF-MS. *Atmos. Meas. Tech.* **14**, 8019–8039 (2021).

29. Thomas, S. J., Li, H., Praplan, A. P., Hellén, H. & Bianchi, F. Complexity of downy birch emissions revealed by Vocus proton transfer reaction time-of-flight mass spectrometer. *Front. For. Glob. Chang.* **5**, 1030348 (2022).

30. Haberstroh, S. *et al.* Terpenoid emissions of two mediterranean woody species in response to drought stress. *Front. Plant Sci.* **9**, 1071 (2018).

31. Li, H. *et al.* Overlooked organic vapor emissions from thawing Arctic permafrost. *Environ. Res. Lett.* **15**, 104097 (2020).

32. Klein, F. *et al.* Characterization of Gas-Phase Organics Using Proton Transfer Reaction Time-of-Flight Mass Spectrometry: Cooking Emissions. *Environ. Sci. Technol.* **50**, 1243–1250 (2016).

33. Jaoui, M., Kleindienst, T. E., Docherty, K. S., Lewandowski, M. & Offenberg, J. H. Secondary organic aerosol formation from the oxidation of a series of sesquiterpenes: α-cedrene, β-caryophyllene, α-humulene and α-farnesene with O3, OH and NO3 radicals. *Environ. Chem.* **10**, 178 (2013).

34. Hellén, H. *et al.* Sesquiterpenes and oxygenated sesquiterpenes dominate the VOC (C5-C20) emissions of downy birches. *Atmos. Chem. Phys.* **21**, 8045–8066 (2021).

35. Luo, Y. *et al.* Oxidation product characterization from ozonolysis of the diterpene ent-kaurene. *Atmos. Chem. Phys.*

22, 5619–5637 (2022).

36. Jokinen, T. *et al.* Production of extremely low volatile organic compounds from biogenic emissions: Measured yields and atmospheric implications. *Proc. Natl. Acad. Sci. U. S. A.* **112**, 7123–8 (2015).

37. Di Carlo, P. *et al.* Missing OH reactivity in a forest: Evidence for unknown reactive biogenic VOCs. *Science (80-.).* **304**, 722–725 (2004).

38. Henrot, A.-J. *et al.* Implementation of the MEGAN (v2.1) biogenic emission model in the ECHAM6-HAMMOZ chemistry climate model. *Geosci. Model Dev.* **10**, 903–926 (2017).

39. Chen, T. & Jang, M. Secondary organic aerosol formation from photooxidation of a mixture of dimethyl sulfide and isoprene. *Atmos. Environ.* **46**, 271–278 (2012).

40. Lee, A. *et al.* Gas-phase products and secondary aerosol yields from the ozonolysis of ten different terpenes. *J. Geophys. Res.* **111**, (2006).

41. Lee, A. *et al.* Gas-phase products and secondary aerosol yields from the photooxidation of 16 different terpenes. *J. Geophys. Res. Atmos.* **111**, D17305 (2006).

42. Pérez, C. *et al.* Atmospheric dust modeling from meso to global scales with the online NMMB/BSC-Dust model – Part 1: Model description, annual simulations and evaluation. *Atmos. Chem. Phys.* **11**, 13001–13027 (2011).

43. Haustein, K. *et al.* Atmospheric dust modeling from meso to global scales with the online NMMB/BSC-Dust model - Part 2: Experimental campaigns in Northern Africa. *Atmos. Chem. Phys.* **12**, 2933–2958 (2012).

44. Jorba, O. *et al.* Potential significance of photoexcited NO2 on global air quality with the NMMB/BSC chemical transport model. *J. Geophys. Res. Atmos.* **117**, (2012).

45. Badia, A. & Jorba, O. Gas-phase evaluation of the online NMMB/BSC-CTM model over Europe for 2010 in the framework of the AQMEII-Phase2 project. *Atmos. Environ.* **115**, 657–669 (2015).

46. Badia, A. *et al.* Description and evaluation of the Multiscale Online Nonhydrostatic AtmospheRe CHemistry model (NMMB-MONARCH) version 1.0: Gas-phase chemistry at global scale. *Geosci. Model Dev.* **10**, 609–638 (2017).

47. Spada, M., Jorba, O., Pérez García-Pando, C., Janjic, Z. & Baldasano, J. M. On the evaluation of global sea-salt aerosol models at coastal/orographic sites. *Atmos. Environ.* **101**, 41–48 (2015).

48. Klose, M. *et al.* Mineral dust cycle in the Multiscale Online Nonhydrostatic Atmosphere Chemistry model (MONARCH) version 2.0. *Geosci. Model Dev.* **14**, 6403–6444 (2021).

49. Guenther, A. *et al.* Estimates of global terrestrial isoprene emissions using MEGAN (Model of Emissions of Gases and Aerosols from Nature). *Atmos. Chem. Phys.* **6**, 3181–3210 (2006).

50. Matsunaga, S. N. *et al.* Determination and potential importance of diterpene (kaur-16-ene) emitted from dominant coniferous trees in Japan. *Chemosphere* **87**, 886–893 (2012).

51. Hiura, T. *et al.* Diversification of terpenoid emissions proposes a geographic structure based on climate and pathogen composition in Japanese cedar. *Sci. Reports 2021 111* **11**, 1–9 (2021).

52. Edtbauer, A. *et al.* Cryptogamic organisms are a substantial source and sink for volatile organic compounds in the Amazon region. *Commun. Earth Environ. 2021 21* **2**, 1–14 (2021).

53. Sindelarova, K. *et al.* Global data set of biogenic VOC emissions calculated by the MEGAN model over the last 30 years. *Atmos. Chem. Phys.* **14**, 9317–9341 (2014).

54. Ma, H. *et al.* The global biogeography of tree leaf form and habit. *Nat. Plants 2023 911* **9**, 1795–1809 (2023).

55. Carlton, A. G., Wiedinmyer, C. & Kroll, J. H. A review of Secondary Organic Aerosol (SOA) formation from isoprene. *Atmos. Chem. Phys. Discuss.* **9**, 8261–8305 (2009).

56. D'Andrea, S. D. *et al.* Aerosol size distribution and radiative forcing response to anthropogenically driven historical changes in biogenic secondary organic aerosol formation. *Atmos. Chem. Phys.* **15**, 2247–2268 (2015).

57. McFiggans, G. *et al.* Secondary organic aerosol reduced by mixture of atmospheric vapours. *Nat. 2019 5657741* **565**, 587–593 (2019).

58. Chen, Q., Li, Y. L., McKinney, K. A., Kuwata, M. & Martin, S. T. Particle mass yield from β-caryophyllene ozonolysis. *Atmos. Chem. Phys.* **12**, 3165–3179 (2012).

59. Gao, L. *et al.* Kinetics, SOA yields, and chemical composition of secondary organic aerosol from β-caryophyllene

ozonolysis with and without nitrogen oxides between 213 and 313â€¯K. *Atmos. Chem. Phys.* **22**, 6001–6020 (2022).

60. Pai, S. J. *et al.* An evaluation of global organic aerosol schemes using airborne observations. *Atmos. Chem. Phys.* **20**, 2637–2665 (2020).

61. Kelly, J. M., Doherty, R. M., O'Connor, F. M. & Mann, G. W. The impact of biogenic, anthropogenic, and biomass burning volatile organic compound emissions on regional and seasonal variations in secondary organic aerosol. *Atmos. Chem. Phys.* **18**, 7393–7422 (2018).

62. Bourtsoukidis, E. *et al.* High temperature sensitivity of monoterpene emissions from global vegetation. *Commun. Earth Environ. 2024 51* **5**, 1–10 (2024).

63. Finessi, E. *et al.* Determination of the biogenic secondary organic aerosol fraction in the boreal forest by NMR spectroscopy. *Atmos. Chem. Phys.* **12**, 941–959 (2012).

64. Krechmer, J. *et al.* Evaluation of a New Vocus Reagent-Ion Source and Focusing Ion-Molecule Reactor for use in Proton-Transfer-Reaction Mass Spectrometry. (2018) doi:10.26434/CHEMRXIV.6502652.V1.

65. Graeffe, F. *et al.* Detecting and Characterizing Particulate Organic Nitrates with an Aerodyne Long-ToF Aerosol Mass Spectrometer. *ACS Earth Sp. Chem.* **7**, 230–242 (2023).

66. Ehn, M. *et al.* A large source of low-volatility secondary organic aerosol. *Nature* **506**, 476–9 (2014).

67. Peräkylä, O. *et al.* Experimental investigation into the volatilities of highly oxygenated organic molecules (HOMs). *Atmos. Chem. Phys.* **20**, 649–669 (2020).

68. Hersbach, H. *et al.* The ERA5 global reanalysis. *Q. J. R. Meteorol. Soc.* **146**, 1999–2049 (2020).

69. Kuenen, J. *et al.* CAMS-REG-v4: a state-of-the-art high-resolution European emission inventory for air quality modelling. *Earth Syst. Sci. Data* **14**, 491–515 (2022).

70. Kaiser, J. W. *et al.* Biomass burning emissions estimated with a global fire assimilation system based on observed fire radiative power. *Biogeosciences* **9**, 527–554 (2012).

71. Xian, P. *et al.* Current state of the global operational aerosol multi-model ensemble: An update from the International Cooperative for Aerosol Prediction (ICAP). *Q. J. R. Meteorol. Soc.* **145**, 176–209 (2019).

72. Yarwood, G., Rao, S., Yocke, M. & Whitten, G. . *Updates to the Carbon Bond Chemical Mechanism: CB05*. (2005).

Supplementary Files

This is a list of supplementary files associated with this preprint. Click to download.

- TableSI2.1and2.2.xlsx
- Supplementaryinformationfinal.pdf